Enhanced joint effects of ENSO and IOD on Southeast China winter precipitation after 1980s

Ling Zhang[1] · Ruizi Shi[1] · Klaus Fraedrich[1,2] · Xiuhua Zhu[3]

Abstract
Based on the NCEP/NCAR reanalysis data, the COBE sea surface temperature (SST) and the GPCC precipitation, the influences of El Niño-South Oscillation (ENSO) on the variability of winter rainfall anomalies in Southeast China is analyzed under the synergistic effect of Indian Ocean Dipole (IOD). Winter precipitation and atmospheric circulation of the years of IOD concurring with ENSO are compared with single IOD or ENSO, to reveal the mechanism of synergistic effects on the variability of winter rainfall anomalies in Southeast China. The results show that the correlation between IOD/ENSO and the winter precipitation in Southeast China has increased since 1980s. These correlations were significant in years of IOD and ENSO co-occurrence compared to years of IOD or ENSO only, which is mainly due to the lagged atmospheric thermal and dynamic responses to an IOD forcing in synergy with ENSO. The positive IOD (PIOD) events can trigger and modify the anticyclone to the east of India, which transports moisture from the tropical Indian Ocean to Southeast China. In addition, El Niño events can strengthen the abnormal anticyclone over Philippines in winter, which is conducive to maintain the water vapor channel from the tropical western Pacific to Southeast China. Information flow analysis shows that the causalities between IOD and ENSO were enhanced after 1980s, causing the significant increase in the frequency of winter abnormal precipitation in the years of IOD and ENSO concurrence. Furthermore, the higher frequency of PIOD with El Niño (compared to negative IOD with La Niña) attained a ratio of 2:1 after the 1980s, enhancing the Southeast China winter precipitation events associated with IOD and ENSO and the generation of interdecadal variability. This study is helpful to understand the mechanisms of winter precipitation changes in Southeast China, and to improve the forecast accuracy of winter extreme precipitation events.

Keywords ENSO · IOD · Winter rainfall in Southeast China · Causality analysis · Climate change

1 Introduction

Southeast China (SEC) is located in East Asian monsoon regions where climate changes have dramatic impacts on social and economic development. Under global warming in the last decades, the frequency of winter extreme precipitation events has increased significantly over South China (Zhi et al. 2010). The frequent natural disasters caused by abnormal precipitation, such as the abnormal snow in southern China during 2008 and 2018, result in considerable loss of life and economy. As important resources of moisture and energy, the Indian Ocean (IO) and the Pacific Ocean play crucial roles in rainfall anomalies over China by influencing the East Asia winter monsoon (Zhang and Sumi 2002; Zhou et al. 2010; Zhang et al. 2015a, 2016a; Xiao et al. 2015). These impacts of the Indian and Pacific Oceans draw our attention to possible mechanisms of the variability of winter

✉ Ling Zhang
lingzhang@nuist.edu.cn

[1] Key Laboratory of Meteorology Disaster, Ministry of Education (KLME)/Joint International Research Laboratory of Climate and Environment Change (ILCEC)/ Collaborative Innovation Center on Forecast and Evaluation of Meteorological Disasters (CIC-FEMD), Nanjing University of Information Science and Technology, Nanjing 210044, China

[2] Max Planck Institute for Meteorology, 20144 Hamburg, Germany

[3] Center for Earth System Research and Sustainability, Hamburg University, 20146 Hamburg, Germany

rainfall in SEC, and to the search of possible predictors of abnormal winter precipitation events.

During the last decades, the increasing trend of abnormal precipitation has been observed in the Yangtze River Basin and southward (Zhai and Zou 2005; Sun and Ao 2013), especially in southeastern coastal areas (Ren et al. 2015). Accordingly, the intensified meridional circulation in the middle and high latitudes with weakened tropical winter monsoon in the lower latitudes plays a major role enhancing the winter precipitation intensity in southern China (Zhi et al. 2010).

The IO has a significant influence on the climate of China. As a well-known coupled ocean–atmosphere phenomenon over the tropical IO, the Indian Ocean Dipole (IOD) is characterized by the aperiodic oscillation of sea surface temperature (SST) between the eastern and western IO (Saji et al. 1999). Previous studies found that a positive IOD (PIOD) event is associated with stronger East Asian summer monsoon, which results in more precipitation over South China during summer and autumn, and vice versa (Qiu et al. 2014). The precipitation anomalies can even extend to boreal winter (Zhang et al. 2014). That is, after the 1980s the lagged atmospheric response to IOD forcing in autumn induces the lasting precipitation anomalies in the subsequent winter, enhancing the correlation between IOD and the winter precipitation anomalies in SEC (Zhang et al. 2016a, b).

IOD is primarily caused by the local ocean–atmosphere interactions, rather than the direct response to external effects such as El Niño-South Oscillation (ENSO); thus, it is usually considered as an independent mode of coupled ocean–atmosphere climate variability (Saji et al. 1999; Webster et al. 1999; Saji and Yamagata 2003; Meyers et al. 2010). However, many analyses have suggested that ENSO plays an important role in triggering IOD events (Baquerobernal and Latif 2002; Saji and Yamagata. 2003; Li et al. 2003; Fischer et al. 2005; Guo et al. 2015; Stuecker et al. 2017). Recent studies have proved that IOD can also modify the amplitude and evolution of ENSO by affecting zonal wind anomalies associated with the Walker circulation (Saji and Yamagata 2003; Li et al. 2003; Kug and Kang 2006; Behera et al. 2006; Luo et al. 2010; Wang et al. 2016; Saji et al. 2018). After removing the spurious oceanic teleconnection, the impact of the IOD on ENSO is as strong as the influence of ENSO on the IOD (Cai et al. 2010).

Recently, it has been proposed that winter rainfall in SEC has a significant correlation with ENSO (Zhang and Sumi 2002; Zhou et al. 2010; Zhang et al. 2015a, b, 2017). Based on the strong mutual impacts between ENSO and IOD, they often occur simultaneously and show synergistic effects on winter precipitation anomalies over SEC (Zhang et al. 2014). These effects are also reflected by two moisture transport channels supplying the abnormal winter precipitation in SEC, which are triggered by PIOD and El Niño, respectively: one originates in the equatorial eastern IO and extends through India and the Bay of Bengal to SEC, while the other is related to the Philippine Sea anticyclone which channels water vapor from western Pacific across the South China Sea into SEC (Zhang et al. 2015a). Moreover, similar to the IOD, the correlation between ENSO and the winter precipitation anomalies in SEC has also increased significantly since the 1980s (Zhou 2011; Li and Hao 2012).

Causes of the increased winter abnormal precipitation in SEC have been discussed focusing on the influence of either IOD or ENSO, while the synergistic effect of IOD and ENSO on this variability has received little attention. Thus, the two following questions need to be answered: first, are there any changes in the connection between IOD and ENSO before and after the 1980s, which lead to the increase of winter rainfall in SEC? Secondly, if there are changes, what are the underlying mechanisms? Based on joint effects of the circulation between ENSO and IOD, the interdecadal variability of winter rainfall anomalies in SEC and its underlying mechanism are investigated. The analysis is structured as follows: data and methods are described in Sect. 2. The space–time interdecadal variability of winter rainfall anomalies in SEC and its relation to ENSO, IOD is evaluated in Sect. 3, and the role of tropical SST anomalies (SSTA) in generating atmospheric response anomalies are analyzed by numerical experiments in Sect. 4; a summary and discussion follows in Sect. 5.

2 Data and methods

2.1 Data

The data utilized are monthly means of SST, atmospheric circulation, and precipitation. The period of analysis covers 66 years from 1951 to 2016. The SST data are obtained from COBE-SST dataset provided by Tokyo Climate Center of WMO Regional Climate Centers in RA II (Asia) with a 1.0°×1.0° resolution (Ishii et al. 2005), and their trends are removed by linear regression eliminating the impact of global climate change. The atmospheric circulation data are taken from the ERA5 datasets with 0.25° ×0.25° resolution. And the Global Precipitation Climatology Centre (GPCC) precipitation data with 1.0° 0× 1.0° resolution (Schneider et al. 2008) are also used. Additionally, the HadISST1 data (Rayner et al. 2003), NOAA Extended Reconstructed SST v5 data (Huang et al. 2017) and monthly precipitation of 160 station observations from the National Meteorology Information Center (https://www.ncc-cma.net/Website/index.php?ChannelID=43&WCHID=5) are applied to further substantiate the relationship between IOD (ENSO) events and precipitation anomalies in SEC.

In our study, ENSO and IOD are measured by the Niño3.4 index and the IOD index (DMI), respectively. The DMI is constructed by the SST anomalies (SSTA) gradient between the western (10° S–10° N, 50° E–70° E) and the eastern (10° S–0°, 90° E–110° E) regions of IO (Saji et al. 1999). Because an IOD event usually begins to develop in summer, peaks in autumn, and decays rapidly in winter (Saji et al. 1999; Webster et al. 1999), only autumn DMI data (calculated by the average SSTA of 3 months from September to November) are used. The monthly Niño3.4 index (derived from ERSST.v5 in winter from December to February) is provided by the NOAA website (http://origin.cpc.ncep.noaa.gov/products/analysis_monit oring/ensostuff/ONI_v5.php). And the "winter year" in this paper is the year to which the December belongs.

2.2 Information flow

In order to investigate the causalities between IOD and ENSO, the method of Liang-Kleeman information flow (Liang 2014) is applied. That is, for any two-time series X_1, X_2, we can get the rate of information flowing from X_2 to X_1:

$$T_{2 \to 1} = \frac{C_{11} C_{12} C_{2,d1} - C_{12}^2 C_{1,d1}}{C_{11}^2 C_{22} - C_{12}^2 C_{11}}, \tag{1}$$

where C_{ij} is the sample covariance between X_i and X_j, and $C_{i,dj}$ is the covariance between X_i and $\widehat{X}_j$. As for $\widehat{X}_j$, denote, for i = 1, 2,

$$\widehat{X}_j(N) = \frac{X_j(N + 1) - X_j(N)}{\Delta t}, \tag{2}$$

where $X_j(N)$ is any element of the time series X_j. Liang (2014) demonstrates that $T_{2 \to 1}$ can be either zero or nonzero. If $T_{2 \to 1}$ is nonzero, the X_2 is causal to X_1. A positive $T_{2 \to 1}$ means that X_2 makes X_1 more uncertain, while a negative $T_{2 \to 1}$ means that X_2 tends to stabilize X_1. In order to test the significance of $T_{2 \to 1}$, the Monte Carlo test (Mudelsee 2010) was applied.

In addition, the empirical orthogonal function (EOF) analysis, sliding correlation, composite analysis, Student's t-test and Fisher's r-to-z transform test are also employed to further characterize the specific interdecadal variability features of winter rainfall anomalies in SEC and the mechanisms with associated circulation anomalies. The water vapor flux was integrated from surface pressure to 300 hPa.

## 3 Effects of IOD and ENSO on precipitation in SEC

Abnormal winter precipitation has increased significantly over SEC in recent decades (Zhi et al. 2010) under global warming (also shown in Fig. 1). In this research, the era of the 1980s is an important demarcation, because the correlation between IOD and SEC winter precipitation is strengthened after the 1980s (Zhang et al. 2016a). Furthermore, the correlation between ENSO and SEC winter precipitation is also enhanced (Zhou 2011; Li and Hao 2012). The increased strength and fluctuation of SEC winter precipitation after the 1980s is demonstrated by the differences of winter precipitation average (Fig. 1a, c) and standard deviation (Fig. 1b, d), which is derived either from GPCC data (Fig. 1a, b) or from observation data of 160 Chinese stations (Fig. 1c, d), revealing positive anomalies over SEC. Based on this interdecadal variability, its possible causes from the perspective of tropical India-Pacific SSTA, are discussed in the following subsections: the changes of the IOD/ENSO-relationship and the precipitation anomalies in SEC are analyzed in Sect. 3.1; the related responses of atmospheric circulation are evaluated in Sect. 3.2.

3.1 Relationships between tropical India-Pacific SST anomalies and precipitation in SEC

As significant positive correlation coefficients between DMI and winter precipitation are mainly located in the southern part of SEC (Zhang et al. 2016a), the precipitation data over this area (105.5° E–120.5° E, 22.5° N–30.5° N) are subjected to further analysis.

First, the interdecadal variability of SEC winter precipitation is characterized by the first EOF of the filtered (9-year running mean: the result indicates the 5th year of the 9-year window) GPCC precipitation, which explains 42.50% of the total variance and exhibits a uniform spatial pattern over SEC (Fig. 2a). The corresponding principal component (PC1) represents a significant increase of winter precipitation after the 1980s (Fig. 2b) with more frequent and stronger precipitation events. Moreover, the results derived from 160 Chinese stations are basically similar (Fig. 2c, d), suggesting the GPCC precipitation data to be reliable.

The 21-year sliding correlation analysis (the coefficient here indicates the 11th year of the 21-year window) is used to reveal the changes in the relationship between IOD/ENSO with winter area-averaged precipitation anomalies in SEC. The link between IOD (DMI from COBE-SST data) and winter precipitation anomalies shows a significant rise in the
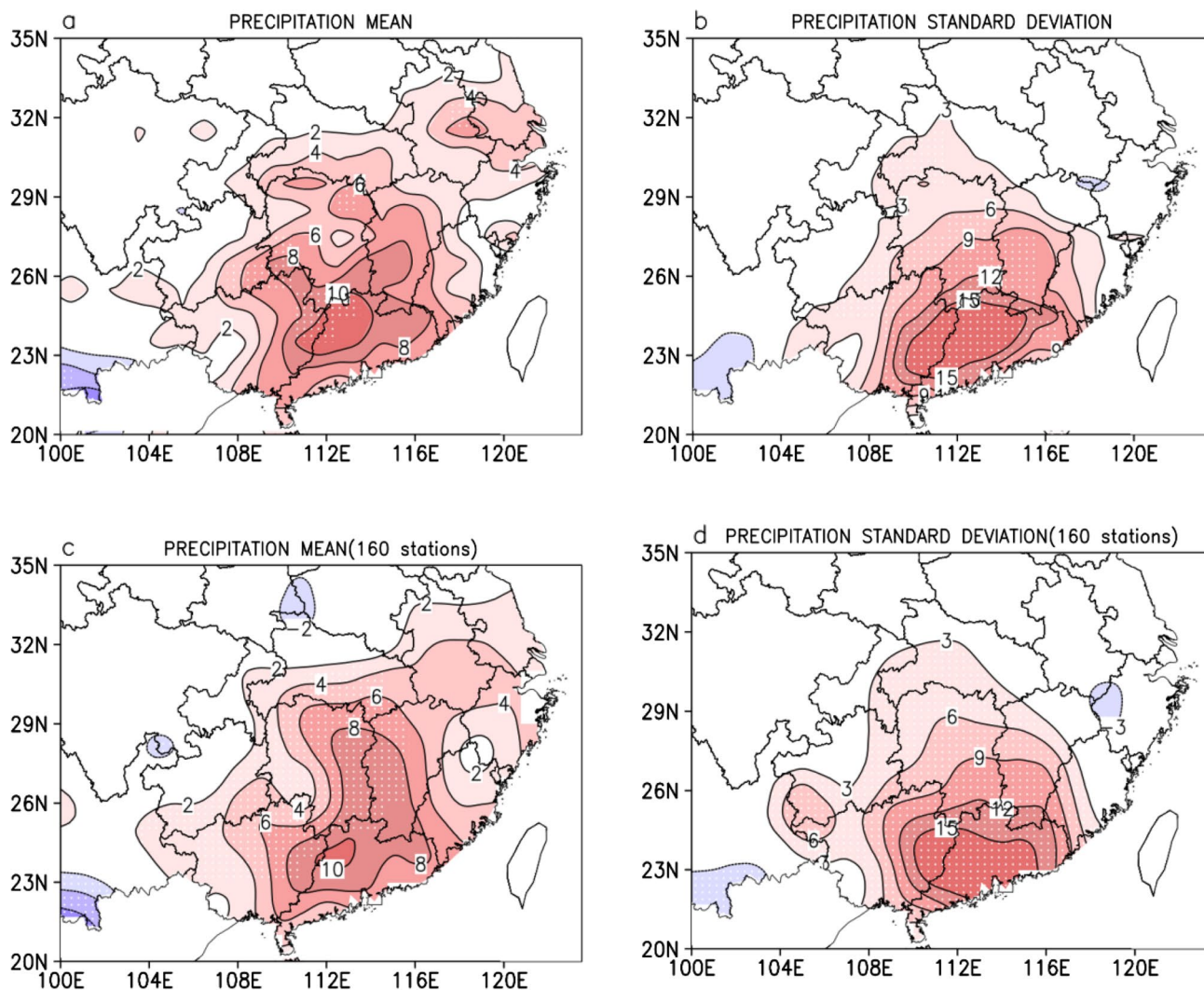
Fig. 1 Difference in winter precipitation fields for average (**a**, **c**) and standard deviation (**b**, **d**) of second (1981–2010) minus first (1951–1980) periods in SEC (mm/month): results of **a**, **b** derived from GPCC precipitation data, **c**, **d** derived from observation data (160 stations). Dotted areas are statistically significant at 90% confidence level

1980s; that is, the correlation attains a higher value exceeding the threshold of statistical significance after the 1980s (black thick line in Fig. 3a). The correlation between ENSO (Niño3.4 from COBE-SST) and winter precipitation anomalies also shows a significant rise since the 1980s, which remains at a high value above the threshold of statistical significance after the 1980s (black thick line in Fig. 3b). In addition, the 31-year sliding correlation coefficients show similar results (Fig. 3c, d; the coefficient here indicates the 16th year of the 31-year window), which indicate that these interdecadal changes are stable. All in all, the sliding correlation analysis indicates that both IOD and ENSO are more strongly correlated with anomalous SEC winter precipitation after the 1980s. The DMI and Niño3.4 from HadISST1 data/NOAA data are also derived to confirm the changing relationship between DMI (Niño3.4) and SEC winter

precipitation anomalies, and shows (blue and red lines in Fig. 3) similar results. In addition, the correlation coefficients between DMI (Niño3.4) and SEC winter precipitation anomalies during 1951–1980 and 1981–2016 were calculated (Table 1), and the significant differences between two correlation coefficients during 1951–1980 and 1981–2016 were tested by Fisher's r-to-z transform test. The results show that correlation coefficients between DMI (Niño3.4) and SEC winter precipitation anomalies during 1981–2016 are much higher than that during 1951–1980. Meanwhile, the correlation coefficients during two sub-period show significant differences, which indicate that these winter interdecadal changes occurring in the 1980s are reliable. Therefore, we select the periods 1951–1980 and 1981–2016 to investigate possible mechanisms of the interdecadal winter precipitation change.
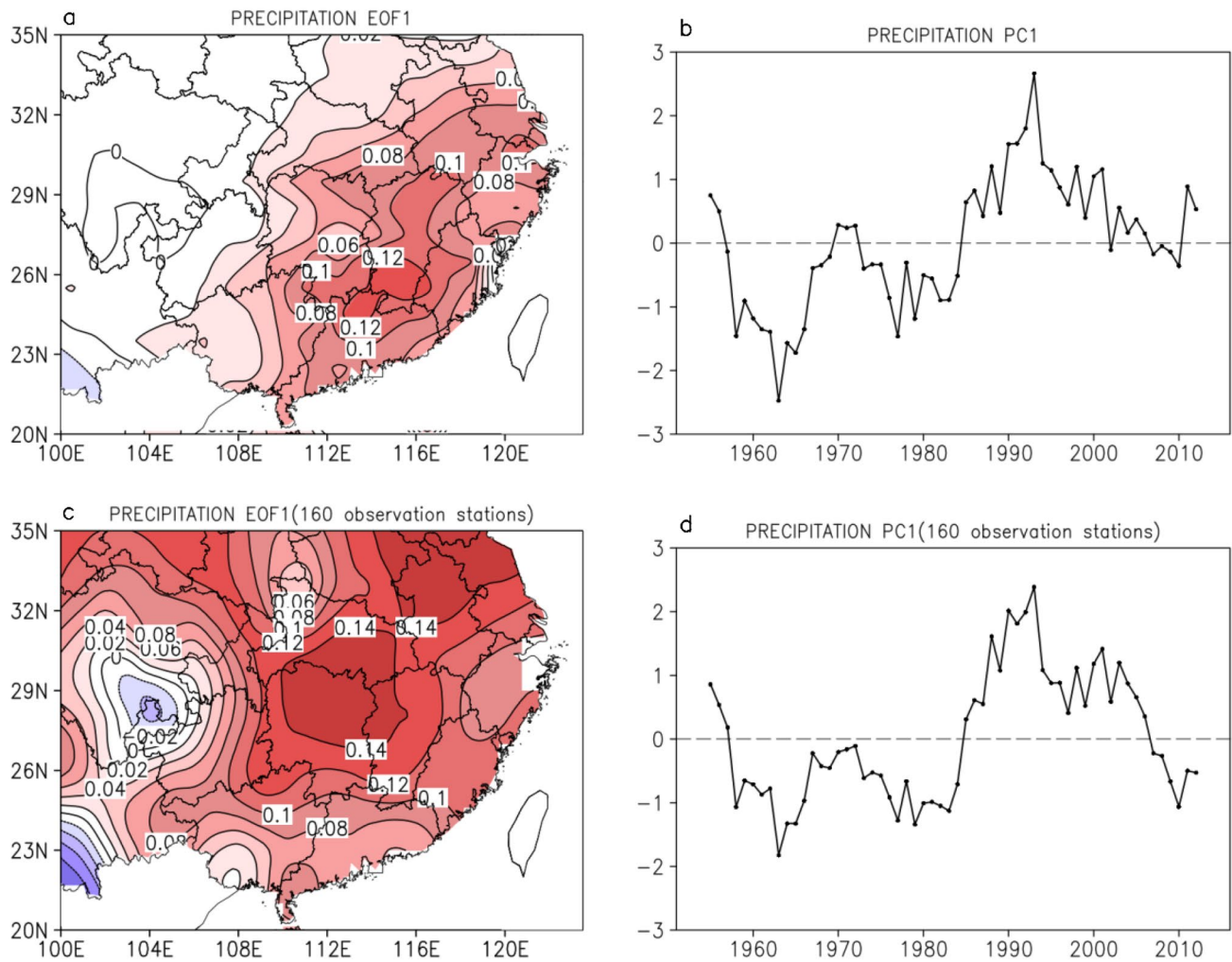
Fig. 2 First EOFs (**a**, **c**) and first principal components (**b**, **d**) of interdecadal variability derived from the filtered (9-year running mean: the result displayed here indicates the fifth year of the 9-year window.) winter precipitation in SEC: results of **a**, **b** derived from GPCC precipitation data, **c**, **d** derived from observation data. PC1 have been normalized, dashed line is the zero line

The relationship changes between IOD and ENSO around 1980s is analyzed using DMI and Niño3.4 index (the time series are shown in Fig. 4a, b). When the normalized Niño3.4 is greater (less) than 1 (− 1), the year is considered to be a typical El Niño (La Niña) year (shown in Table 2 and Fig. 4b with marked years); when normalized DMI (COBE-SST) is greater (less) than 1 (− 1), the year is considered to be a typical PIOD (NIOD) year (shown in Table 3 and Fig. 4a with marked years). Table 2 shows that there are five El Niño years from 1951 to 1980, and two of them are companied by PIOD, whereas from 1981 to 2016 there are seven El Niño years, four of which are companied by PIOD. The frequency of El Niño accompanied by PIOD increased from 40% of the total before the 1980s to 57% of the total after the 1980s. Furthermore, similar results are shown in Table 3, in which the frequency of PIOD accompanied by El Niño increased from 50% of the total before the 1980s

to 67% of the total after the 1980s. These data indicate that the frequency of El Niño and PIOD concurrence has significantly increased since the 1980s. However, the frequency of La Niña and NIOD concurrence shows few changes. The ratio of PIOD with El Niño to NIOD with La Niña is 4-to-2 after the 1980s. Furthermore, in Fig. 4c the time series of normalized area-averaged winter precipitation in SEC indicates more precipitation in the years of PIOD with El Niño than the single PIOD or El Niño years.

To clarify the change of relationship between ENSO and IOD and the corresponding influence on winter precipitation in SEC, causality-analysis is applied (Liang 2014). In order to keep the number of years in both periods consistent, here we use 1951–1980 and 1981–2010 to calculate the information flows. Figure 5 shows the information flows from autumn Niño3.4 to the SST over IO. In the tropical IO, there are positive anomalies covering
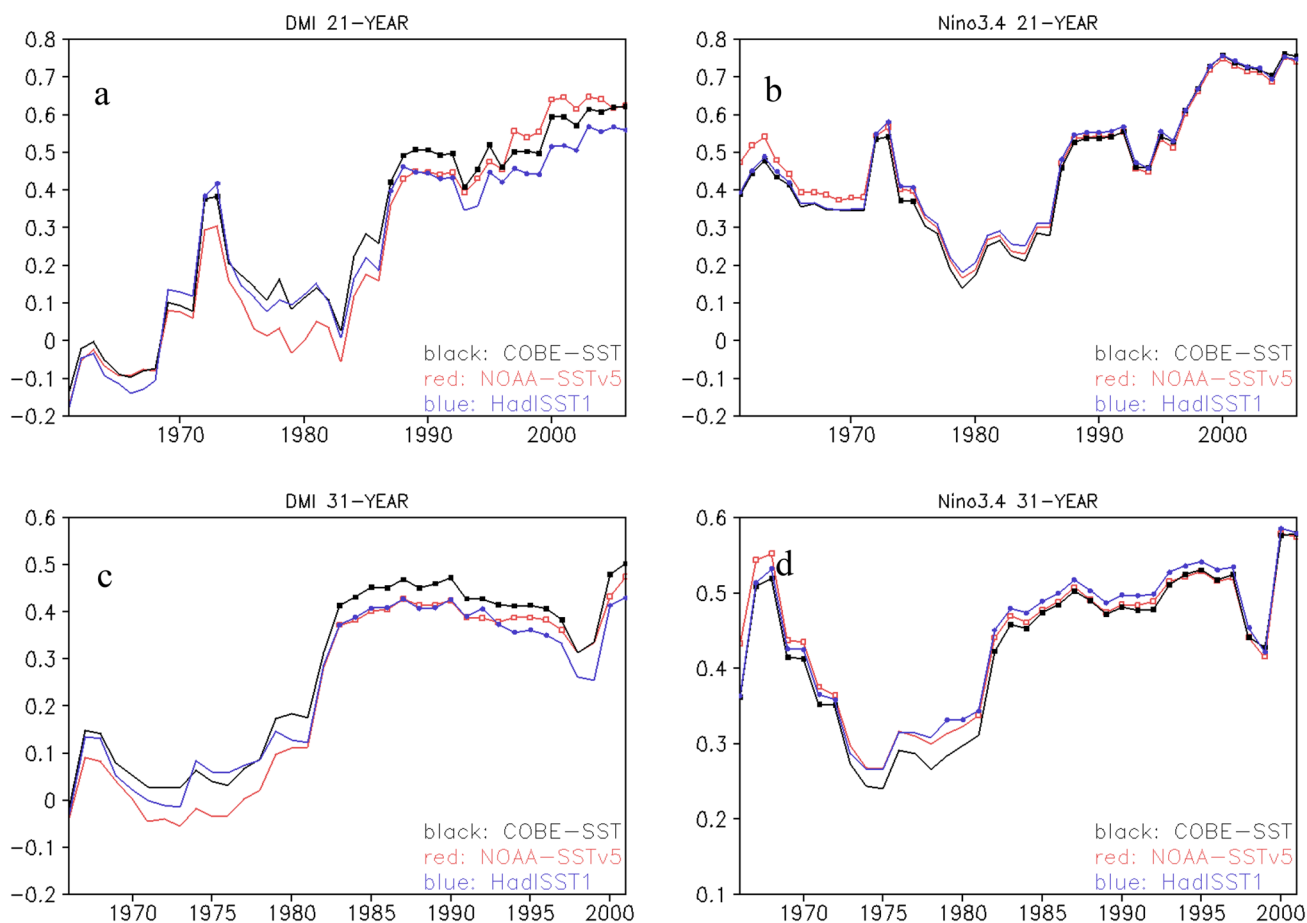
Fig. 3 21-year/31-year sliding correlation coefficients between DMI (**a, c**)/Niño3.4 (**b, d**) and area-averaged winter precipitation in Southeast China: black line derived from COBE-SST data, blue line derived from HadISST1 data, red line derived from NOAA Extended Reconstructed SST v5 data; for **a** and **b** the sliding correlation coef- ficient displayed here indicates the 11th year of the 21-year window; for **c** and **d** the sliding correlation coefficient displayed here indicates the 16th year of the 31-year window. Markers are statistically signifi- cant at 90% confidence level with efficient degrees of freedom

Table 1 The correlation coefficients between DMI/Nino3.4 indices and area-averaged winter precipitation in SEC during 1951–1980 and 1981– 2016, */** represents statistically significant at 95% confidence level for Student's t-test/ Fisher's r-to-z transform test

	DMI			Nino3.4		
	COBE-SST	NOAA-SSTV5	HadISST1	COBE-SST	NOAA-SSTV5	HadISST1
1951–1980	− 0.02	− 0.04	− 0.04	0.36	0.43*	0.36
1981–2016	0.49*	0.44*	0.41*	0.57*	0.57*	0.58*
Z	− 8.36**	− 7.61**	− 7.16**	− 4.18**	− 2.84**	− 4.33**

the northwest region before the 1980s (Fig. 5a). Then the positive anomalies retreat westward with negative anomalies appearing at the eastern coast after the 1980s (Fig. 5b), which enhance the dipole-like flow pattern. And the absolute value of information flow from DMI index in fall to Niño3.4 index in winter (Table 4) has significantly increased after the 1980s, which illustrate that the link between IOD events and ENSO events enhanced after the

1980s. Furthermore, Table 4 shows the information flows from DMI (Niño3.4) to area-averaged winter precipitation in SEC before and after 1980s, in which the information flows both from IOD to winter precipitation in SEC and from ENSO to winter precipitation in SEC are enhanced after the 1980s. In addition, their values after the 1980s are positive, indicating that both IOD and ENSO affect winter precipitation in SEC more uncertain. Hence, we
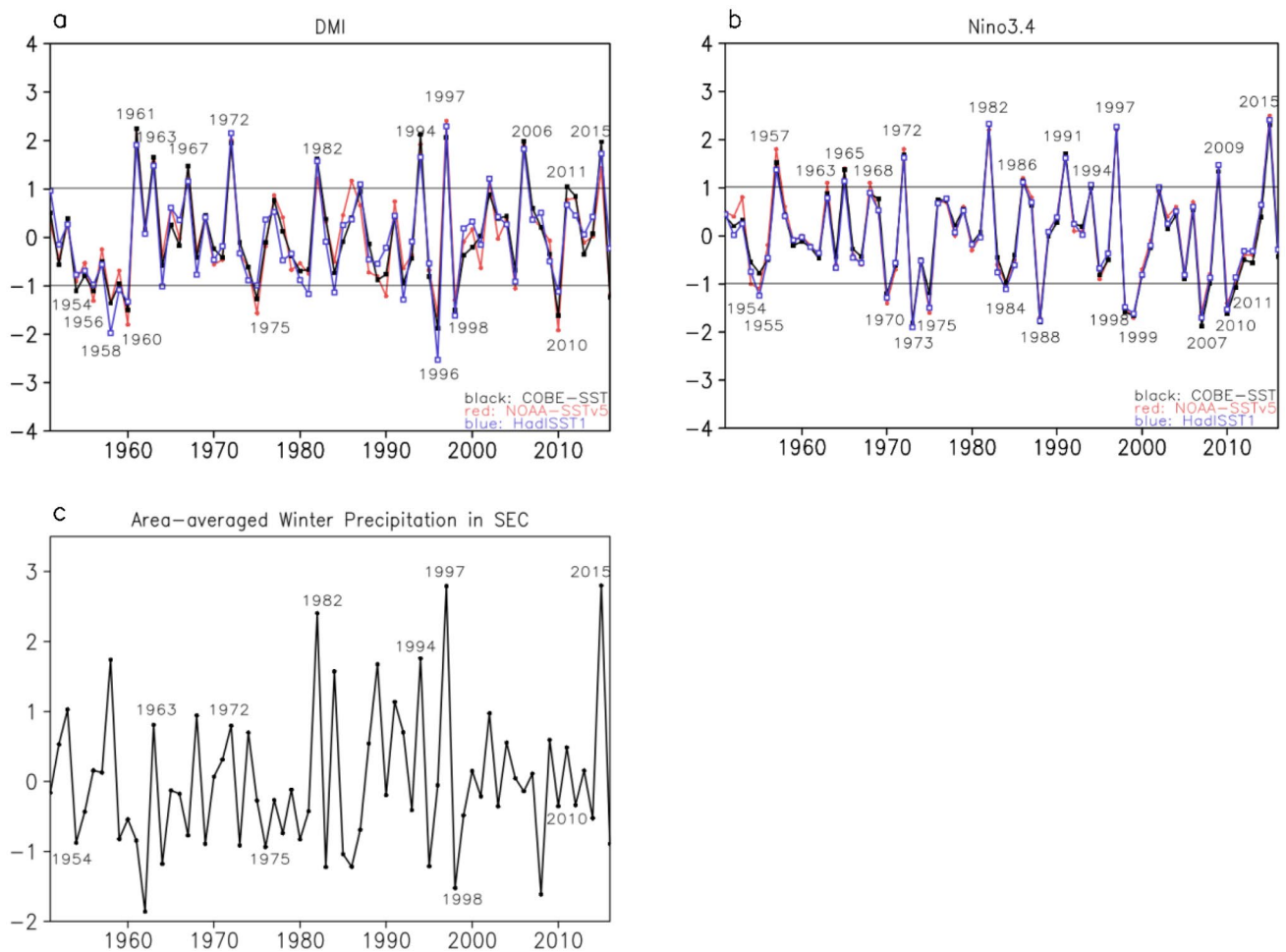
Fig. 4 Normalized DMI (**a**)/Nino3.4 (**b**)/area-averaged winter precipitation in SEC (**c**) in 1951–2016. The typical IOD years and ENSO years are marked in the **a** and **b**, respectively. PIOD with El Niño years and NIOD with La Niña years are marked in the **c**

Table 2 Years of ENSO events; *P, N, S* represent PIOD, NIOD, and single ENSO years, respectively. E is El Niño event and L is La Niña event

Before 1980s						
E	1957(S)	1963(P)	1965(S)	1968(S)	1972(P)	
L	1954(N)	1955(S)	1970(S)	1973(S)	1975(N)	
After 1980s						
E	1982(P)	1986(S)	1991(S)	1994(P)	1997(P)	2009(S)	2015(P)
L	1984(S)	1988(S)	1998(N)	1999(S)	2007(S)	2010(N)	2011(P)

Table 3 Years of IOD events; *E, L, N* represent El Niño, La Niña, and normal years, respectively. PIOD is positive IOD event and NIOD is negative IOD event

| Before 1980s					
PIOD	1961(N)	1963(E)	1967(N)	1972(E)	
NIOD	1954(L)	1956(N)	1958(N)	1960(N)	1975(L)
After 1980s					
PIOD	1982(E)	1994(E)	1997(E)	2006(N)	2011(L)	2015(E)
NIOD	1996(N)	1998(L)	2010(L)		
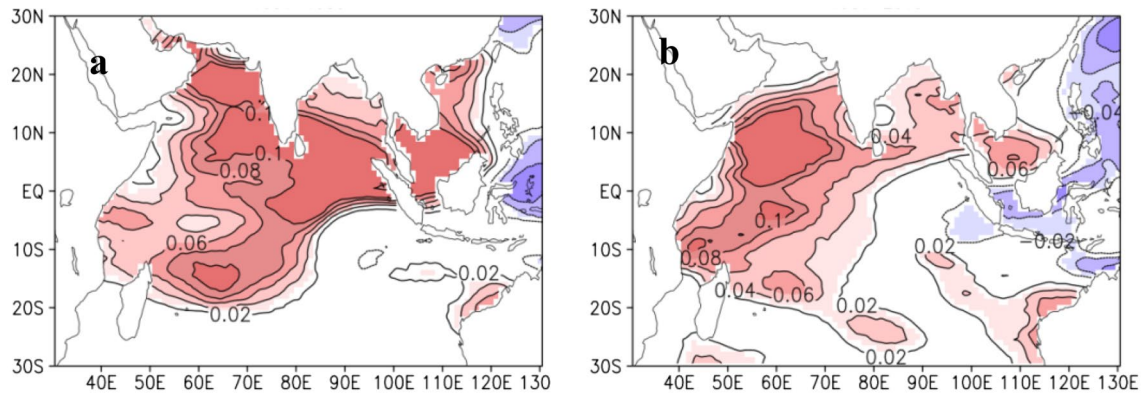
Fig. 5 Information flow (nats/month) from Niño3.4 in boreal fall (September to November) to tropical Indian Ocean SST simultaneously: **a** 1951–1980, **b** 1981–2010. Shaded areas are statistically significant at 95% confidence level

Table 4 Information flows (nats/month) in winter before and after the 1980s (the asterisk means statistically significant at 90% confidence level): **a** from DMI to area-averaged winter precipitation in SEC, **b** from Niño3.4 to area-averaged winter precipitation in SEC and **c** from DMI in fall to Niño3.4 index in winter

	DMI → pre in SEC	Niño3.4 → pre in SEC	DMI → Niño3.4
1951–1980	-2.49E-02*	1.91E-02*	-4.12E-02*
1981–2010	2.53E-02*	8.61E-02*	-8.62E-02*

infer that there is an increased certainty of winter precipitation anomalies in SEC, only when IOD and ENSO occur in pairs.

To prove the strong winter precipitation anomalies in SEC is a result of the combined influence of ENSO and IOD, composites of winter precipitation anomalies in six kinds of different events are shown in Fig. 6 based on Tables 2 and 3. For simplicity, in the following, a single PIOD (NIOD) /El Niño (La Niña) is referred to as SP (SN)
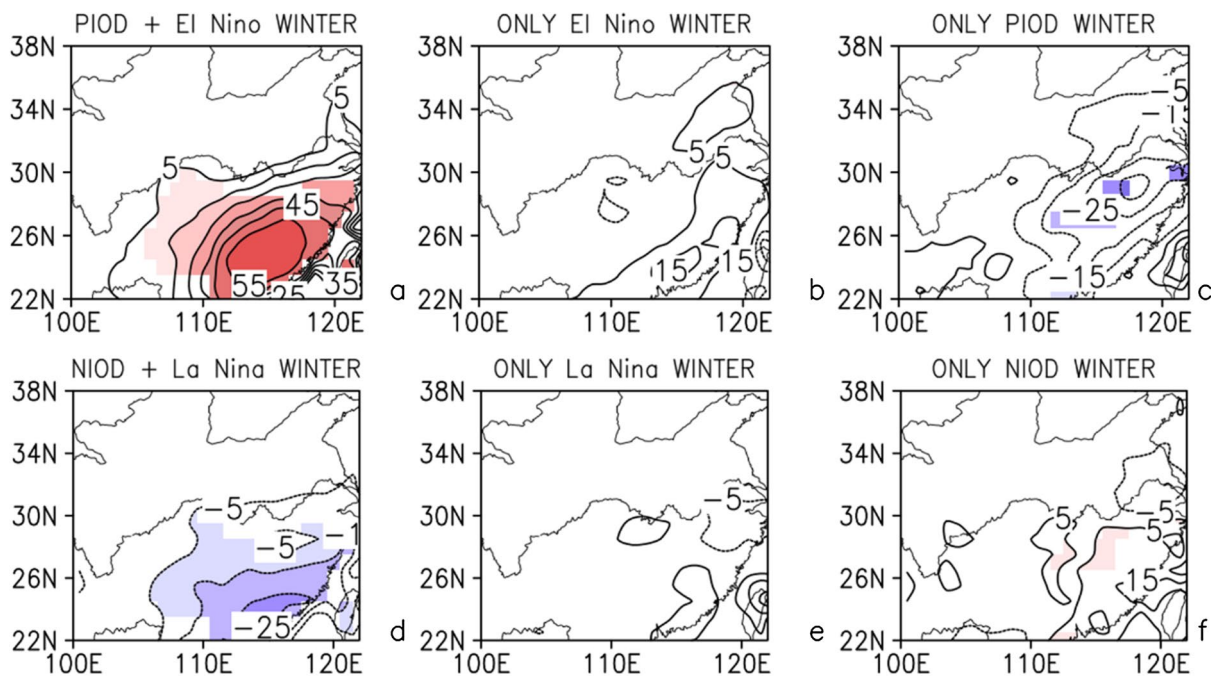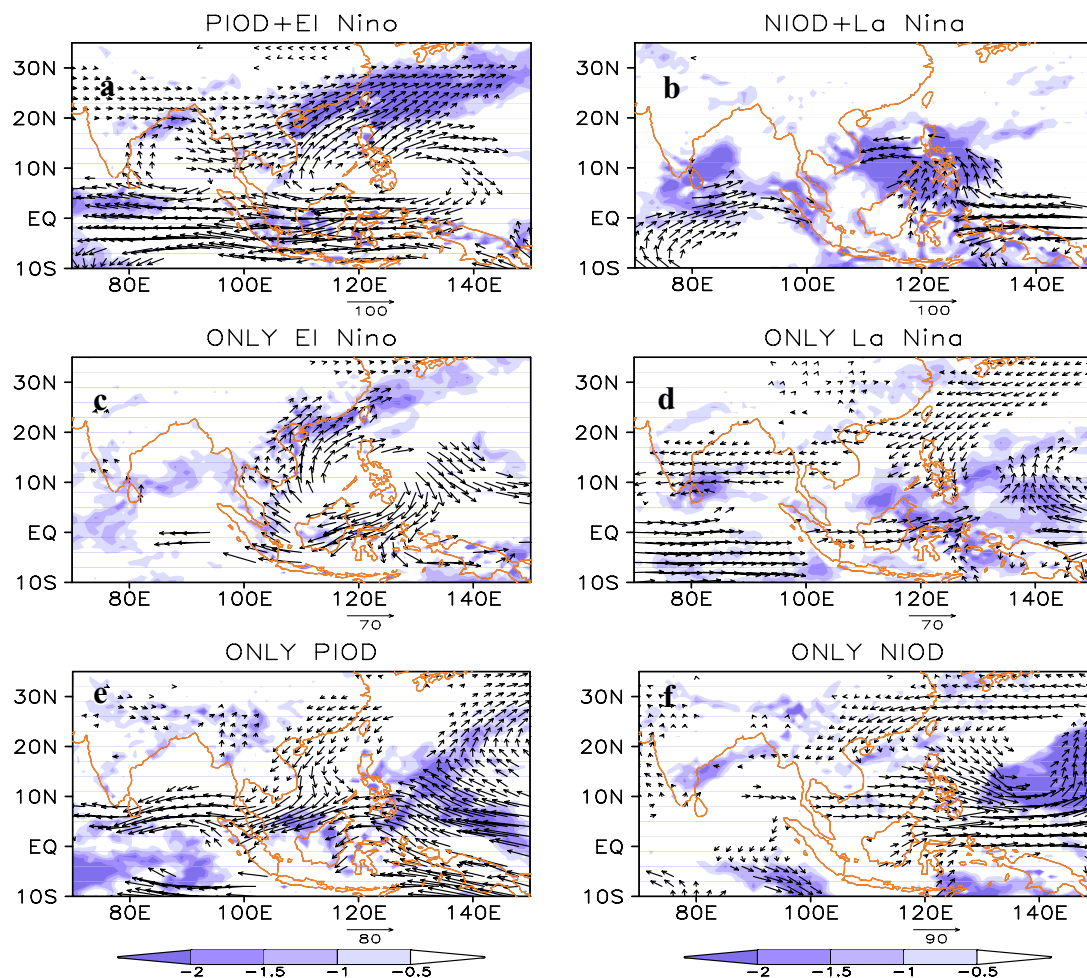

Fig. 6 Composites of winter precipitation anomalies (mm/month) in 1951–2016: **a** positive IOD events and El Niño events concurrence years, **b** single El Niño anomalous years, **c** single positive IOD anomalous years, **d** negative IOD events and La Niña events concurrence years, **e** single La Niña anomalous years, **f** single negative IOD anomalous years. Shaded areas are statistically significant at 90% confidence level

/SE (SL) and a PIOD (NIOD) with El Niño (La Niña) is referred to as PE (NL). The purpose of composites here is to investigate the difference between the influence of PE (NL) and SP (SN) /SE (SL) on SEC winter precipitation, which can explain why the increase of PE after the 1980s leads to an increase of winter precipitation in SEC. Considering the numbers of samples, the whole period data from 1951 to 2016 are employed in this section. In Fig. 6, the significant positive precipitation anomalies appear only in PE years (Fig. 6a), and the maximum value exceeds 55 mm/month. While the positive anomalies in SE years (Fig. 6b) are weak, and the anomalies in SP years (Fig. 6c) even turn into negative. Similar results are shown for the negative phase (Fig. 6d–f): the significant negative precipitation anomalies only can be found in NL years (Fig. 6d),

whereas the minimum value is slightly weaker and around − 25 mm/month. These composites of winter precipitation indicate that neither single El Niño (La Niña) nor single PIOD (NIOD), but their combined effects can lead to significant positive (negative) anomalous winter precipitation in SEC. Therefore, after the 1980s the increased frequency of IOD and ENSO concurrence, especially the increased frequency of PIOD with El Niño (Tables 2, 3), leads to more frequent occurrences of abnormal winter rainfall events in SEC, which finally leads to the significant increase of winter precipitation in SEC after the 1980s. How does the atmospheric circulation anomaly respond during PE years? These will be explained in the next subsection to further clarify that the increased frequency of PIOD with El Niño has an effect on the winter precipitation increasing in SEC after 1980s.


Fig. 7 Composites of seasonal mean anomalies of vertical integral of water vapor flux (kg/(m s); arrows) and its divergence (10⁻² g/(m² s); shading) in winter during 1951–2016: **a** positive IOD events and El Niño events concurrence years, **b** negative IOD events and La Niña events concurrence years, **c** single El Niño anomalous years, **d** single La Niña anomalous years, **e** single positive IOD anomalous years, **f** single negative IOD anomalous years. The arrows and shading areas shown are statistically significant at 90% confidence level

3.2 Responses of atmospheric circulation

To investigate how the tropical India-Pacific SST anomalies influence the abnormal winter precipitation in SEC, the anomalies of tropospheric moisture transport and Walker circulation during the PE (NL), the SE (SL), and the SP (SN) years are subjected to composite analysis, which reveals the following results: (1) During the PE years, the composites of

the vertically integrated water vapor flux in winter (Fig. 7a) show two water vapor channels. One of them depends on the abnormal easterlies over the eastern Indian Ocean near the equator, which turn northward over the Indian continent and merge with westerly anomalies over the Bay of Bengal into SEC. This channel conveys abundant moisture from the tropical IO. The other one relies on the anti-cyclonic circulation over the South China Sea–Philippines Sea, which
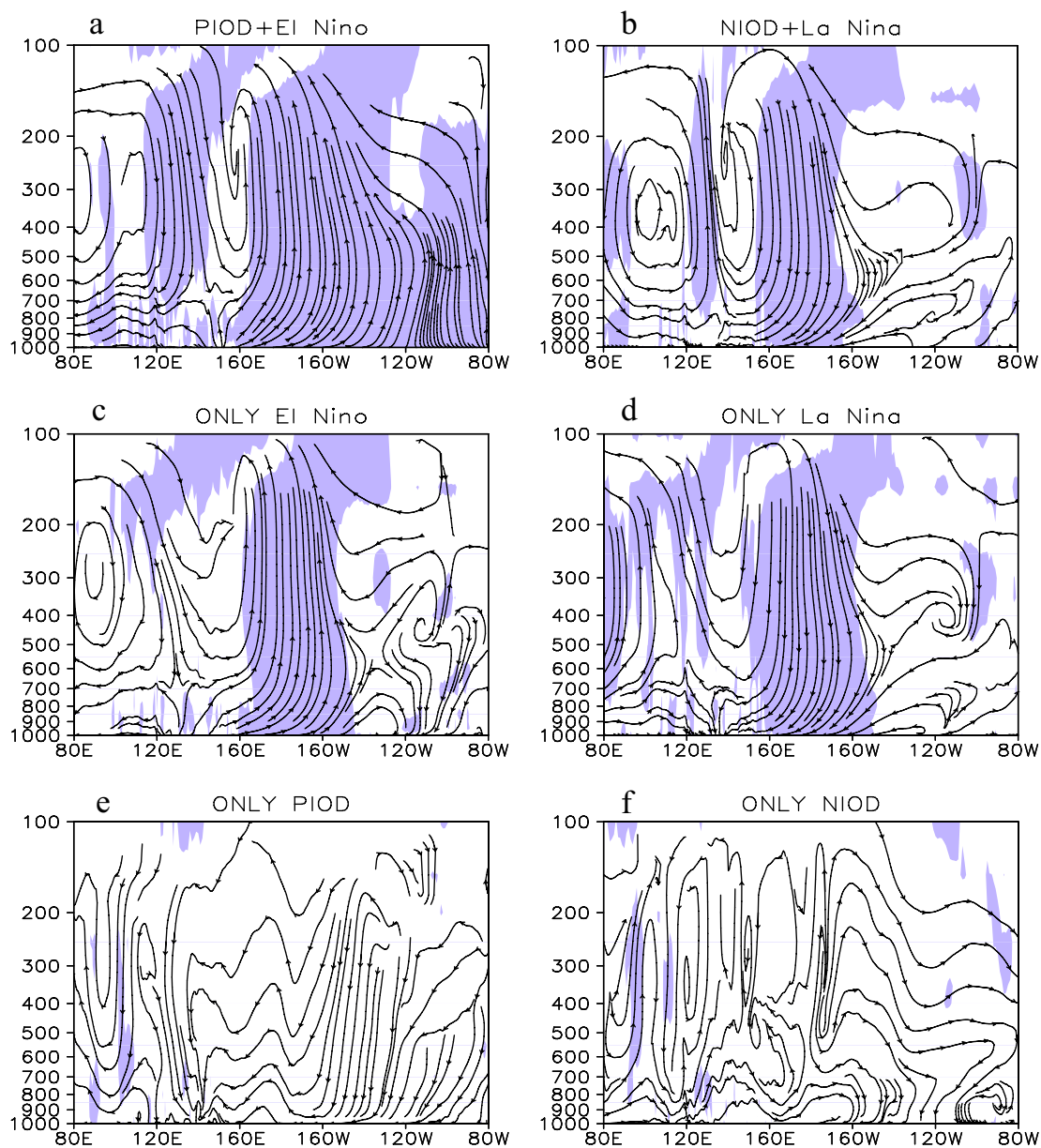
Fig. 8 Composites of the meridional-height section of longitude mean of zonal wind anomalies (U, m/s) and vertical velocity anomalies (W, Pa/s) along (10°S to equator) in winter of 1951–2016: **a** positive IOD events and El Niño events concurrence years, **b** negative IOD events and La Niña events concurrence years, **c** single El Niño

anomalous years, **d** single La Niña anomalous years, **e** single positive IOD anomalous years, **f** single negative IOD anomalous years. Shaded areas are statistically significant at 90% confidence level. Vertical velocity is multiplied with −100 to get positive results with adjustment to the U scale

transports moisture to SEC from Maritime Continents and adjacent seas. (2) Furthermore, the Walker circulation over Pacific is weakened, characterized by anomalous ascending motion over central Pacific and descending motion over western Pacific. Over the tropical IO, an anti-Walker circulation occurs with descending (ascending) motion over Eastern (Western) IO, leading to abnormal easterlies over equator of IO (Fig. 8a). (3) In winter, due to the lagged atmospheric response to IOD forcing and the synergistic effect of El Niño, the abnormal Walker circulation and the easterlies remain. The anti-cyclonic circulation moves to the Philippines Sea and southwesterly prevails over SEC (Fig. 7a). All of these phenomena contribute to a strong moisture convergence over SEC in the PE years.

The water vapor channel to the east India is induced by the abnormal SST during the PIOD events, that is, the Eastern IO cooling excites Rossby waves which, in agreement with the Gill Model (Zhang et al. 2015a, b), excite the low level anti-cyclonic circulation over India. While the other water vapor channel over South China Sea–Philippine Sea is mainly induced by the El Niño pattern with the positive thermodynamic feedback of western North Pacific cooling due to a decrease of local convective heating (Wang 2002). In addition, recent studies indicate that, similar to El Niño, also the PIOD can trigger and intensify the South China Sea–Philippine Sea anticyclone in autumn, because the distribution pattern and the SSTA evolvement benefit the formation of the horizontal asymmetry of moisture and temperature anomalies as well as the large-scale divergence anomaly over the maritime continent, which are the main reasons of this anticyclone's development (Li et al. 2010; Kim and An 2019). Whereas, without the synergistic effect, the anticyclone under the single PIOD or El Niño events is weaker and decays rapidly. Moreover, its characteristic eastward movement from the southern South China Sea to the Philippine Sea has disappeared (Li et al. 2010, 2015).

During the SE years, the South China Sea–Philippines Sea anticyclone's location is more westward than in PE years, whereas the easterlies over equator of the eastern IO and the anticyclone over the Bay of Bengal are weaker (Fig. 7c). Furthermore, the ascending motion over the central-eastern Pacific and the descending motion over eastern IO are also weaker than in PE years, with reduced extent and strength (Fig. 8c). Thus, in the SE years, although the anticyclone over South China Sea–Philippines Sea contributes to the moisture convergence over SEC, the positive anomalies of winter precipitation hardly pass the significance test (Fig. 6b). During the SP years (Figs. 7e, 8e), although a weak anti-cyclonic circulation remains over India, the anti-Walker circulations and abnormal easterlies do not generate over the equator of IO. Without anti-cyclonic circulation observed over the Philippines Sea, the SEC is dominated by abnormal north-easterly winds in winter, leading moisture divergence appears in the

SP years. The negative phases have similar results with drier winter in SEC (Figs. 7b, d, f, 8b, d, f). Since the focus of this research is mainly on the positive phases, the details of these situations will not be discussed here.

In summary, during PE years, the two abnormal anti-cyclonic circulations over Bay of Bengal and the South China Sea–Philippines Sea can be lasted from autumn to subsequent winter, leading to abundant moisture transports to SEC from equatorial IO and tropical western Pacific and formatting abnormal positive precipitation. Under these atmospheric responses to the SSTA of PIOD and El Niño concurrence, the increasing precipitation in SEC is resulted from the high frequency of concurrence events of PIOD and El Niño after 1980s. The mechanisms of the abnormal atmospheric circulation responses to the SSTA of PIOD and El Niño concurrence in winter were investigated by composite analysis, which would be further confirmed by numerical study in the next section.

4 IOD and ENSO forcing of winter precipitation anomalies in SEC: an idealized model experiment

A tropical IO and Pacific forcing experiment with Planet Simulator (PlaSim; Fraedrich et al. 2005) general circulation model is employed to assess the contribution of SST anomalies in the tropical IO and Pacific to drive water vapor channels for winter precipitation anomalies in SEC. A climatological global Atmospheric Model Intercomparison Project (AMIP) SST with annual cycle is applied as tropical SST forcing in the control run. The last 30 years of a 50 years control run were used in this study. The model is capable of reproducing realistic climatological water vapor flux in autumn and winter (Fig. 9a, b). As shown in Fig. 9a, b, the simulated vertical integral of water vapor flux bears qualitative similarities with the counterparts of the NCEP/NCAR reanalysis data (Fig. 9c, d).

The sensitivity experiment has run 30 years with the same set up after a spin-up time with abnormal tropical SST added to the climatological SST forcing. The SST anomalies forcing are shown in Fig. 10, which are derived from the composites of monthly SST anomalies of the HadISST1 data during concurrence years of PIOD & El Niño (Table 2, Fig. 10a, c). Since the amplitudes of the tropical Pacific SST anomaly are 4–6 times that of the SST anomaly in the Indian Ocean, the SST anomalies are processed by formula (3) to balance the atmospheric responses to SST anomalies in the tropical Pacific and Indian Ocean.

$$\text{sstanew}(i, j, t) = \sqrt{\text{ssta}(i, j, t)} \times 2, \qquad (3)$$

where $\text{ssta}(i, j)$ is the SST anomalies during concurrence years of PIOD & El Niño events according to the Table 2
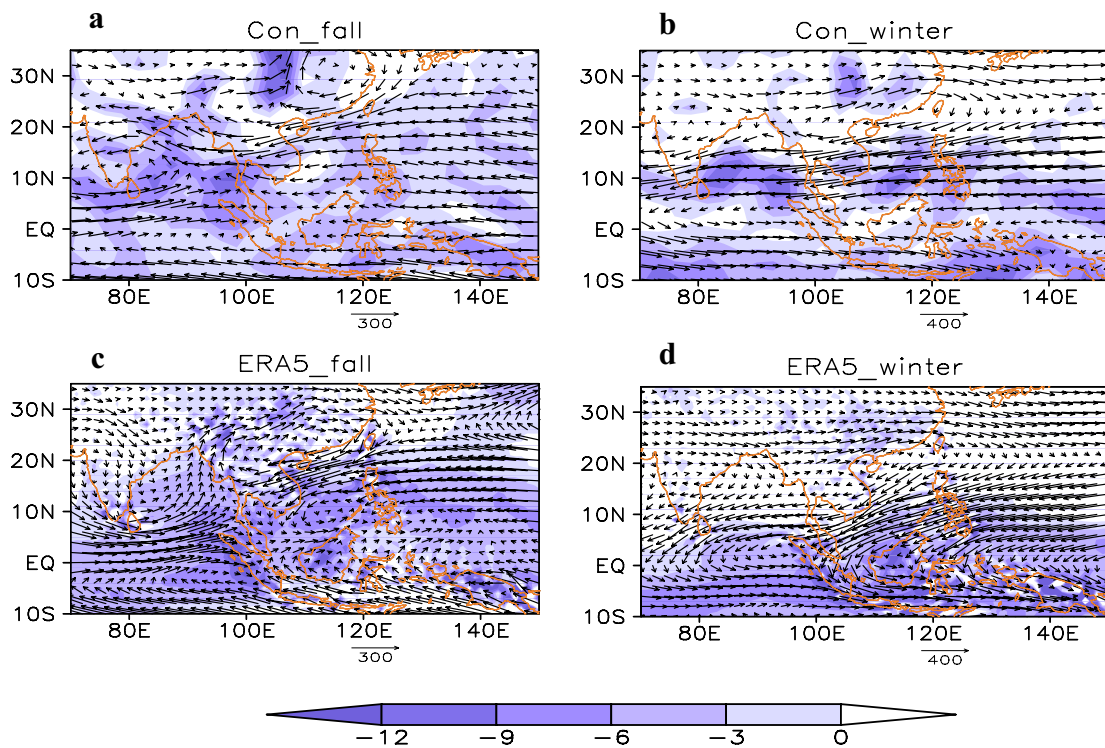
Fig. 9 The climatology mean of vertical integral of water vapor flux (kg/(m s); arrows) in autumn (**a, c**) and winter (**b, d**): **a, b** the simulated results in control experiment, **c, d** composite results from (1981–2010) ERA5 datasets
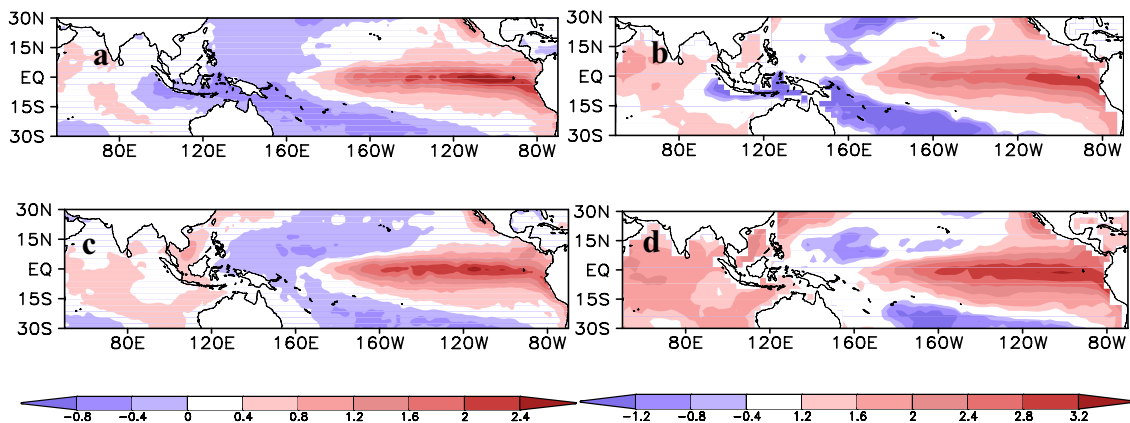

Fig. 10 The abnormal tropical SST (℃) in autumn (**a, b**) and winter (**c, b**) in the observations and (**a, c**) sensitive experiment (**b, d**)

and the sstanew(i,j,t) represent the new constructed SST anomalies in the sensitive experiment. The SST anomalies (Fig. 10) show that the PIOD reaches its maximum amplitude in autumn and decays dipole mode in winter, while the El Niño develops in autumn and peaks in winter (Fig. 10a, c). Under these forcing conditions, the results are compared with the control run as shown in Fig. 11. In autumn, two water vapor channels, which correspond to anticyclones over Bay of Bengal and South China Sea–Philippine Sea, bring abundant water vapor from tropical eastern IO and

tropical western Pacific to the eastern China (Fig. 11a, c), respectively. In addition, during winter these water vapor channels still exist, whereas the South China Sea–Philippine Sea anticyclone move southward and strengthen (Fig. 11b, d). As a result, the water vapor transport can only reach as far as SEC and no longer extend further northward in winter.

According to the velocity potential and zonal wind anomalies in the sensitive experiment (Fig. 12), anti-Walker circulation anomalies are captured with abnormal easterlies (westerlies) over equatorial eastern Indian Ocean (western
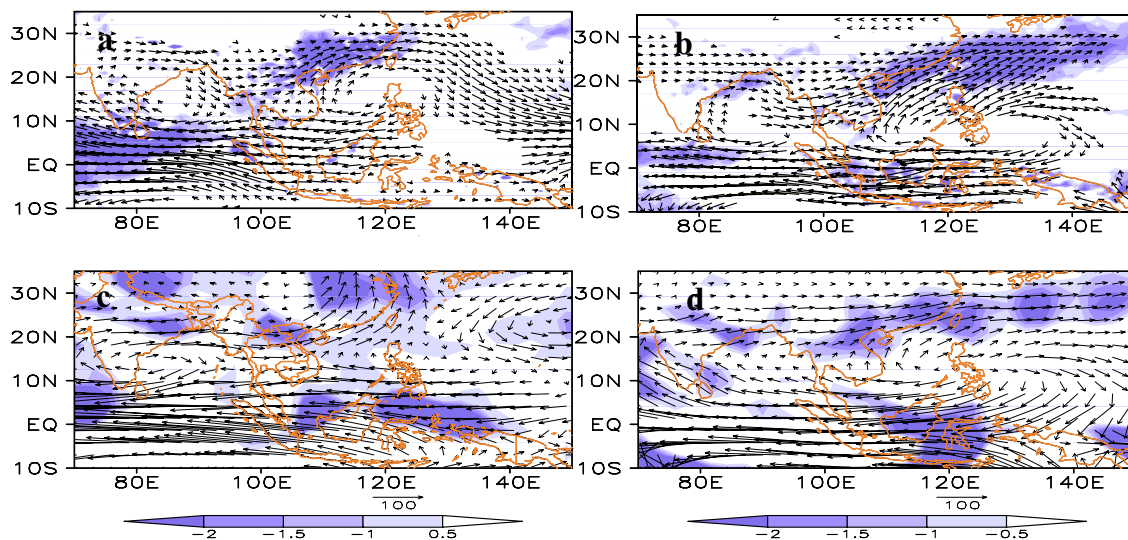
Fig. 11 The abnormal vertical integral of water vapor flux (kg/(m s); arrows) and its divergence (10^{-2}g/(m^2 s); shading) in autumn (**a, c**) and winter (**b, d**): **a, b** the anomalies during positive IOD events and

El Niño events concurrence years in Era5 datasets, **c, d** the differences between sensitivity experiment and control run
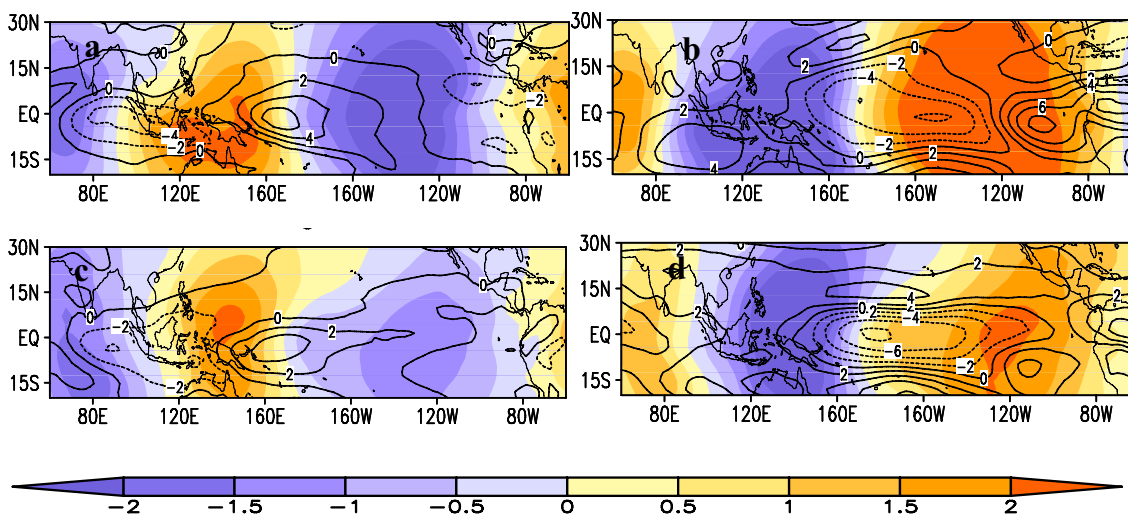
Fig. 12 The difference between sensitivity experiment and control run of zonal wind (contour, m/s) and velocity potential function (shading, m^2/s) at 850 hPa (**a, c**) and 300 hPa (**b, d**) in autumn (**a, b**) and winter (**c, d**)

Pacific) at low levels of troposphere (Fig. 12a, c) and with abnormal westerlies (easterlies) over equatorial eastern Indian Ocean (western Pacific) at high levels of troposphere (Fig. 12b, d) in the autumn and winter. These results are quite different from the simulation of Wang et al. (2000). In their simulation, under the forcing of SST anomalies of a single El Niño, there is a weaker anomalous anticyclone over the Philippine Sea in winter, whereas the easterlies over tropical eastern IO are too weak to produce a significant anticyclone over Bay of Bengal, leading to negative winter precipitation anomalies in SEC. These differences indicate

that, although the IOD decays in winter, the associated time-lagged atmospheric response still exists. After the 1980s, with enhanced intensity of IOD events and prolonged heating anomalies in winter (Zhang et al. 2016a, b), the lagged atmospheric responses of IOD strengthen the synergistic link with ENSO, which agrees well with the changes described by the information flow (Sect. 3.1).

In summarizing, the two water vapor channels, which are associated with the winter precipitation anomalies in SEC, are induced by anomalous tropical SST forcing during ENSO and IOD concurrence years. During the El Niño

and PIOD years, abundant moisture is transported from the equatorial eastern IO and the western Pacific to South China across North India and the Bay of Bengal and the South China Sea, which are modulated by anti-cyclonic circulation anomalies over east India and over the South China Sea–Philippine Sea, respectively. These background circulations generate favorable patterns for enhancing the precipitation anomalies as observed. The numerical experiments further proved that the high frequency events of concurrence events of PIOD and El Niño after 1980s had positive contributions to the increasing winter precipitation after 1980s in SEC.

5 Conclusion and discussion

5.1 Conclusion

Based on the change of the connections between ENSO and IOD, this paper explores the interdecadal variability of winter rainfall in SEC during the last 66 years and its underlying mechanism. The space–time interdecadal variability of winter rainfall in SEC is captured by the first EOF of the 9-year running mean precipitation data provided by GPCC; the relationships with IOD and ENSO events are investigated through sliding correlation analysis and causality analysis employed to the COBE-SST global sea surface temperature data set. Additionally, the features of the associated circulation fields are derived from NCEP/NCAR reanalysis data employing composite analysis; the results

are further substantiated by numerical experiments with a global circulation model and abnormal tropical SST forcing. The key results are followed and the schematic diagram is presented in Fig. 13.

The winter precipitation in SEC has significantly increased since the 1980s, which is accompanied by the enhanced correlation between IOD/ENSO and winter precipitation in SEC. And the information flow results show that the frequency of ENSO and IOD concurrence especially El Niño and PIOD concurrence has significantly increased due to the enhanced causalities linking IOD and ENSO after the 1980s (higher yellow values in Fig. 13 after 1980s), which play an important role in the increasing winter precipitation in SEC after 1980s.

The composite and numerical studies show the mechanisms of the abnormal atmospheric circulation responses to the SSTA of PIOD and El Niño concurrence. During the winter of positive IOD and El Niño (NIOD and La Niña) co-occurrence years, significant positive (negative) precipitation anomalies are observed in SEC due to the anomalous anticyclones lasted from autumn to winter over east India and South China Sea–Philippine Sea. Two water vapor channels (green arrows in Fig. 13) lead to abundant moisture convergence in the eastern China: the one originates from tropical eastern IO, along the northwest boundary of abnormal anticyclone over east India, through Bay of Bengal; the other one from tropical western Pacific, along the northwest boundary of abnormal anticyclone over South China Sea–Philippine Sea, through South China Sea, inducing positive precipitation anomalies in
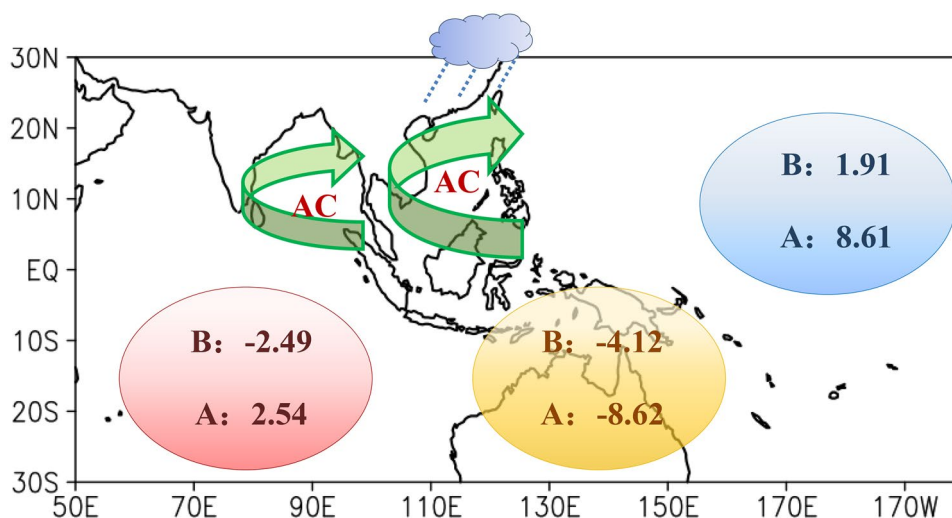
Fig. 13 The information flows between different indices and water channels which are associated with winter precipitation anomalies in SEC. The values in the red (blue) shaded areas indicate the information flows (10^{-2} nats/month; statistically significant at 90% confidence level) from DMI in fall (Niño3.4 index in winter) to area-averaged winter precipitation in SEC. The yellow values are the information flows from DMI in fall to Niño3.4 index in winter. *B, A* respectively correspond to the value before the 1980s and that after the 1980s. Green arrows indicate the water vapor channels in winter. *AC* represents the anomalous anticyclone

SEC. Whereas under the forcing of single El Niño or single PIOD, the positive precipitation anomalies in winter are weak or disappeared, due to the lack of common maintenance of two water vapor channels.

Therefore, the significant increase in the frequency of PIOD and El Niño concurrence is beneficial to maintain the water vapor channels in winter. Finally, these persistent water vapor channels increased the winter precipitation in SEC after the 1980s.

5.2 Discussion

In our study, we divide the abnormal typical SST years into six categories based on whether the positive (negative) IOD and El Niño (La Niña) are linked to each other or not. However, there are also some special years, such as the 2011, which shows PIOD with La Niña (Table 3). Moreover, the winter precipitation in these special years does not completely conform to the conclusions, which we have illustrated. For example, the precipitation of 2011 (not shown) shows small-scale positive winter anomalies in SEC, although the fields of SST, Walker circulation and tropospheric moisture transport all coincide with the flow pattern of La Niña events, which indicates the possible existence of other mechanisms. Furthermore, Zhang et al. (2016b) suggested that the two kinds of El Niño have different effects on IOD. They found that there is a strong correlation between the magnitudes of the Eastern Pacific (EP) El Niño and the IOD, whereas the relationship between Central Pacific (CP) El Niño and IOD is more dependent on the zonal location of the SST anomalies but not on their magnitudes. Wang (2016) further proposed that the CP El Niño exhibits more antagonistic (but not synergistic) effects on autumn precipitation in South China when it appears jointly with IOD. In this paper we did not discuss the difference between the two types of El Niño on winter precipitation in SEC. However, during 1994 with CP El Niño and PIOD concurrence, the positive SST anomalies of PIOD pattern is situated further westward than normal, and strong negative precipitation anomalies are observed over SEC in fall, turning into positive anomalies in winter (not shown). This requires further effort to investigate the more comprehensive mechanisms of winter rainfall's interdecadal variability in SEC by applying coupled climate models.

References

Baquerobernal A, Latif M (2002) On dipole-like variability in the tropical Indian Ocean. J Clim 15(11):1358–1368

Behera SK, Luo JJ, Masson S et al (2006) A CGCM Study on the Interaction between IOD and ENSO. J Climate 19(19):1688–1705

Cai W, Sullivan A, Cowan T (2010) Interactions of ENSO, the IOD, and the SAM in CMIP3 models. J Clim 24(6):1688–1704

Fischer AS, Terray P, Guilyardi E et al (2005) Two independent triggers for the Indian Ocean Dipole/zonal mode in a coupled GCM. J Clim 18(17):3428–3449

Fraedrich K, Jansen H, Krik E, Luksch U, Lunkeit F (2005) The planet simulator: towards a user friendly model. Meteorol Z 14(3):299–304

Guo F, Liu Q, Sun S et al (2015) Three types of Indian Ocean dipoles. J Clim 28(8):3073–3092

Huang B, Thorne PW, Banzon VF et al (2017) NOAA extended reconstructed sea surface temperature (ERSST), Version 5. NOAA National Centers for Environmental Information 2017

Ishii M, Shouji A, Sugimoto S et al (2005) Objective analyses of sea-surface temperature and marine meteorological variables for the 20th century using ICOADS and the Kobe collection. Int J Climatol 25(7):865–879

Kim JW, An SI (2019) Western north Pacific anticyclone change associated with the El Nino–Indian Ocean dipole coupling. Int J Climatol 39:2505–2521

Kug JS, Kang IS (2006) Interactive feedback between ENSO and the Indian Ocean. J Clim 19(9):1784–1801

Li C, Hao M (2012) Relationship between ENSO and winter rainfall over Southeast China and its decadal variability. Adv Atmos Sci 29(6):1129–1141

Li T, Wang B, Chang CP et al (2003) A theory for the Indian Ocean dipole-zonal mode. J Atmos Sci 60(17):2119–2135

Li Y, Wang Y, Zhu W et al (2010) A study of the effects of anomalous SSTs over the tropical Indian Ocean and the tropical Pacific on the establishment of the anomalous Philippine Sea anticyclone. Acta Meteorol Sin 68(6):865–876 (**in Chinese with English abstract**)

Li Y, Wang Q, Mu L et al (2015) Different evolutions of the Philippine sea anticyclone for the impact of El Niño in peak phases with and without a positive Indian ocean dipole. J Trop Meteorol 21:23–33

Liang XS (2014) Unraveling the cause-effect relation between time series. Phys Rev E Stat Nonlinear Soft Matter Phys 90(5–1):052150

Luo JJ, Zhang RC, Behera SK et al (2010) Interaction between El Niño and abnormal Indian Ocean dipole. J Clim 23(3):726–742

Meyers G, Mcintosh P, Pigot L et al (2010) The Years of El Niño, La Niña, and Interactions with the Tropical Indian Ocean. J Clim 20(20):2872–2880

Mudelsee M (2010) Climate time series analysis. Springer, Dordrecht

Qiu Y, Cai W, Guo X et al (2014) The asymmetric influence of the positive and negative IOD events on China's rainfall. Sci Rep 4(4):4943

Rayner NAA, Parker DE, Horton EB et al (2003) Global analyses of sea surface temperature, sea ice, and night marine air temperature since the late nineteenth century. J Geophys Res Atmos. https://doi.org/10.1029/2002jd002670

Ren Z, Zhang M, Wang S et al (2015) Changes in daily abnormal precipitation events in South China from 1961 to 2011. J Geogr Sci 25(1):58–68

Saji NH, Yamagata T (2003) Structure of SST and surface wind variability during indian ocean dipole mode events: COADS observations. J Clim 16(16):2735–2751

Saji NH, Goswami BN, Vinayachandran PN et al (1999) A dipole mode in the tropical Indian Ocean. Nature 401(6751):360

Saji NH, Jin DH, Thilakan V (2018) A model for super El Nino. Nat Commun. https://doi.org/10.1038/s41467-018-04803-7

Schneider U, Fuchs T, Meyer-Christoffer A et al (2008) Global precipitation analysis products of the GPCC. Global Precipitation Climatology Centre (GPCC), DWD, Internet Publication, p 112

Stuecker MF, Timmermann A, Jin FF et al (2017) Revisiting ENSO/ Indian Ocean dipole phase relationships. Geophys Res Lett 44:2481–2492

Sun JQ, Ao J (2013) Changes in precipitation and abnormal precipitation in a warming environment in China. Chin Sci Bull 58(12):1395–1401

Wang B (2002) Pacific-East Asian teleconnection, part II: how the Philippine Sea anticyclone established during development of El Niño. J Clim 15(22):3252–3265

Wang Y (2016) The physical relationship between the two types of El Niño and IOD and its impacts on the autumn rainfall in China. Dissertation, Nanjing University of Information Science & Technology (in Chinese)

Wang B, Wu R, Fu X (2000) Pacific-East Asian teleconnection: how does ENSO affect East Asian climate? J Clim 13(9):1517–1536

Wang H, Kumar A, Murtugudde R (2016) Interaction between the Indian Ocean Dipole and ENSO associated with ocean subsurface variability. NOAA: Science and Technology Infusion Climate Bulletin: 41st NOAA Annual Climate Diagnostics and Prediction Workshop 1–5. https://www.weather.gov/media/sti/climate/STIP/41CDPW/41cdpw-HWang.pdf

Webster PJ, Moore AM, Loschnigg JP et al (1999) Coupled ocean–atmosphere dynamics in the Indian Ocean during 1997–98. Nature 401(6751):356–360

Xiao M, Zhang Q, Singh VP (2015) Influences of ENSO, NAO, IOD and PDO on seasonal precipitation regimes in the Yangtze River basin, China. Int J Climatol 35(12):3556–3567

Zhai PM, Zou XK (2005) Changes in temperature and precipitation and their impacts on drought in China during 1951–2003. Adv Clim Change Res 1(1):16–18 (in Chinese)

Zhang R, Sumi A (2002) Moisture circulation over East Asia during El Niño Episode in Northern winter, spring and autumn. J Meteorol Soc Jpn Ser II 80(2):213–227

Zhang XL, Xiao ZN, Li YF (2014) Effects of Indian Ocean SSTA with ENSO on winter rainfall in China. J Trop Meteorol 20(1):45–56 (in Chinese with English abstract)

Zhang L, Sielmann F, Fraedrich K et al (2015a) Variability of winter abnormal precipitation in Southeast China: contributions of SST anomalies. Clim Dyn 45(9–10):2557–2570

Zhang R, Li T, Wen M et al (2015b) Role of intraseasonal oscillation in asymmetric impacts of El Niño and La Niña on the rainfall over southern China in boreal winter. Clim Dyn 45(3–4):559–567

Zhang L, Sielmann F, Fraedrich K et al (2016a) Atmospheric response to Indian Ocean Dipole forcing: changes of Southeast China winter precipitation under global warming. Clim Dyn 48(5–6):1–16

Zhang W, Wang Y, Jin F et al (2016b) Impact of different El Niño types on the El Niño/IOD relationship. Geophys Res Lett 42(20):8570–8576

Zhang RH, Min QY, Jingzhi SU (2017) Impact of El Niño on atmospheric circulations over East Asia and rainfall in China: Role of the anomalous western North Pacific anticyclone. China Earth Sci 60(6):1–9

Zhi XF, Zhang L, Pan JL (2010) An analysis of the winter abnormal precipitaion events on the background of climate warming in southern China. J Trop Meteorol 16(4):325–332

Zhou LT (2011) Interdecadal change in sea surface temperature anomalies associated with winter rainfall over South China. J Geophys Res Atmos. https://doi.org/10.1029/2010JD015425

Zhou LT, Chiyung T, Zhou W et al (2010) Influence of South China Sea SST and the ENSO on winter rainfall over South China. Adv Atmos Sci 27(4):832–844

Publisher's Note Springer Nature remains neutral with regard to jurisdictional claims in published maps and institutional affiliations.